

Dynamical Observation of Femtosecond-Laser-Induced Bubbles in Water Using a Single Laser Source for Probing and Sensing

Dhirendra Tiwari¹, Yves Bellouard^{1*}, Andreas Dietzel^{1,2}, Maosheng Ren², Eric Rubingh², and Erwin Meinders²

¹Micro- and Nano-Scale Engineering, Mechanical Engineering, Eindhoven University of Technology, Den Dolech 2, 5612 AZ Eindhoven, The Netherlands
²Holst Centre/TNO, PO BOX 8550, 5605 KN Eindhoven, The Netherlands

Received August 9, 2010; accepted October 28, 2010; published online November 26, 2010

We report on dynamical observations of femtosecond-laser-generated bubbles in water using a single-laser-source pump/probe setup combined with stroboscopic imaging. With this simple setup, we accurately measure the transmission of a probe beam and simultaneously record images giving the size and lifetime of single-pulse-generated bubbles. Our experiments indicate that stable bubble nucleation can be obtained with pulses repetition rate up to 142 kHz, which offers promising perspectives for high-throughput jetting. © 2010 The Japan Society of Applied Physics

DOI: 10.1143/APEX.3.127101

Femtosecond lasers are characterized by ultrashort duration pulses (typically 10^{-13} s), which when focused, lead to extremely high instant power density (in our case, the order of magnitude is 10 GW/cm^2). These extreme conditions induce nonlinear absorption phenomena like multi-photon absorption processes¹⁾ that can be a precursor for plasma formation in transparent media.^{2,3)} In liquids, under certain energy and focusing conditions, femtosecond laser pulses can lead to the formation of bubbles.⁴⁾ The controlled laser-induced nucleation of bubbles is particularly interesting for precision microsurgery⁴⁻⁷⁾ and liquid transfer processes involving jet formation.⁸⁾ Due to the nonlinear nature of the fluid–laser interaction, femtosecond pulses offer a means to generate bubbles anywhere in a water volume. In the case of the femtosecond laser radiation, the mechanism of bubble formation is essentially photoacoustically driven as compared with thermally driven phenomena observed with laser emitting longer pulses.⁴⁾ The appearance of bubbles prior to a jetting event is ubiquitous in experiments⁸⁾ involving fluid excitation through the impact of liquids on solids,¹¹⁾ solids on liquid- or fluid-like sand,¹²⁻¹⁴⁾ liquids on liquids, and amplitude overdriven oscillating liquid surface.¹⁵⁻¹⁸⁾ In fact, the controlled bubble nucleation followed by collapse close to the liquid–air¹⁹⁾ or liquid–solid²⁰⁾ interface forms liquid jets. Recently, a few authors have reported liquid jet formation at liquid–air interface.²¹⁻²⁶⁾ However, the mechanism of jet formation remains elusive.

In this letter, the dynamics of single femtosecond laser pulse induced bubbles is presented. In particular, we investigate the maximum repetition rate for the controlled formation of cavitation bubbles in water using femtosecond laser pulses. We use an optical probe to examine the laser–liquid interaction zone combined with stroboscopic imaging information. Further, we report on the validity of a single pulse-single bubble process up to a repetition rate of 870 kHz.

Figure 1 shows the experimental setup for the time resolved study of laser generated bubbles. We use a single femtosecond laser source to generate both a pump and a probe beam. The laser source emits 380 fs-pulses at 1030 nm and at a frequency of 9.4 MHz (Amplitude Systèmes t-Pulse 500). Using an acousto optic modulator (AOM), the pump laser beam is extracted at various repetition rates (1 Hz up to

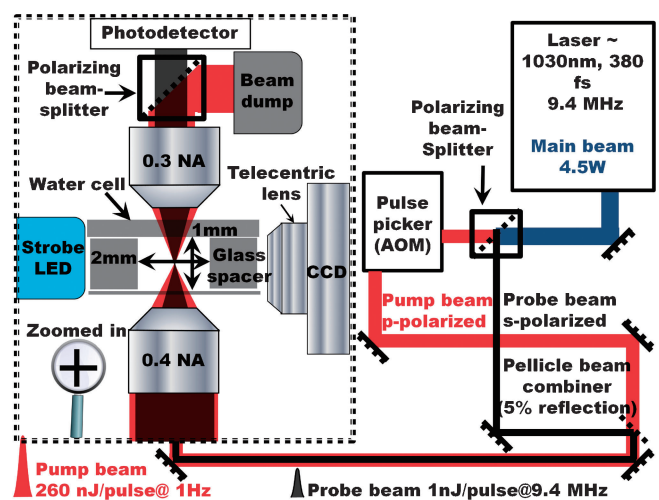


Fig. 1. Laser setup for time-resolved study of laser-induced bubble dynamics in water cell. The pump and the probe beams originate from the same laser source. The pump beam repetition rate is varied using an AOM, while the probe beam has a constant repetition rate of 9.4 MHz. The two beams follow the same optical path so that they are collinear and confocal at the water cell (left side of the drawing). Pump and probe beams are collected and later separated by a polarizing beam splitter. This forward-transmitted “probe signal” is sampled through a fast photo detector. Orthogonal to the laser propagation axes, the stroboscopic shadow imaging system consists of a pulsed LED and a CCD mounted on a 20x telecentric lens.

870 kHz) from the main beam. The pump beam is then focused at a depth of $500 \mu\text{m}$ inside a water cell using a 0.40 numerical aperture (NA) objective lens (OFR-Thorlabs). The water cell, shown in Fig. 1, is a 12.5-mm-long, 2-mm-wide, and 1-mm-thick channel formed by the precise assembly of two microscope glass slabs (with polished edges) sandwiched between a cover slip ($200 \mu\text{m}$ thick) and a microscope slide (1 mm thick) both made of fused quartz in order to prevent unwanted interactions with the laser beam. To probe the laser focal region, a second laser beam sampled from the same laser source is used. This beam is collected just before the AOM and therefore has the same repetition rate as that of the oscillator (9.4 MHz). This probe beam gives us a time resolution of 106 ns. Its pulse energy is less than 1.0 nJ so that no interaction with the liquid is observed. The probe beam optical path is adjusted so that it gets collinear and confocal with the pump beam at the water cell. To separate them, the two beams have two different

*E-mail address: y.bellouard@tue.nl

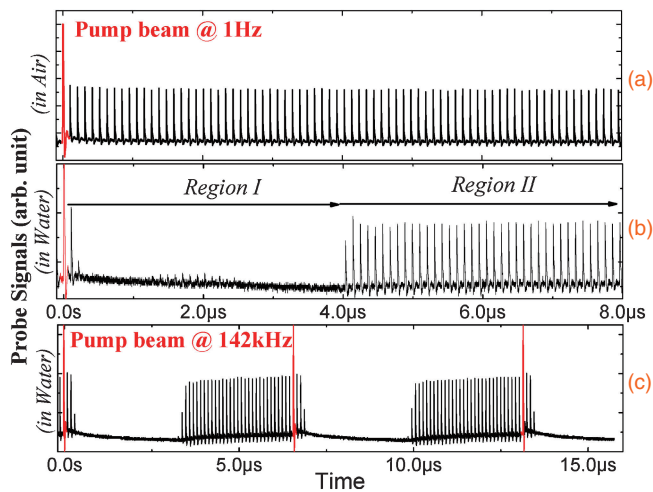


Fig. 2. Typical forward transmitted optical signal obtained in: (a) an empty water cell (i.e., in air), and (b) a filled water cell. The red pulse represents the attenuated pump pulse and the black ones correspond to the probe beam pulses emitted at 9.4 MHz (i.e., 106 ns time separation between consecutive pulses). The pump-pulse-generated bubble obstructs the probe signal transmission for about 4 μ s. (c) Optical probe signal observed at 142 kHz pump pulse repetition rate. The black pulses are the probe beam pulses with 106 ns as the consecutive pulses separation. The probe pattern follows the pump pulse frequency and the time-scale of the dip in the probe signal is similar to the one observed in the single pulse event.

polarization states, perpendicular one to another. After passing through the water cell, the two beams are collected by a 0.3 NA objective lens and later, separated using a Glan polarizer beam splitter. The probe beam is then sampled on a fast-photodiode (rise time and fall time are 3.3 and 15.5 ns, respectively). Signals are observed with a LeCroy wave-surfur oscilloscope. Figures 2(a) and 2(b) shows two typical probe chronograms, obtained for an empty and a filled water cell, respectively. In both cases, the first high amplitude pulse (indicated with the red color) corresponds to the attenuated pump pulse while the low amplitude pulses are the probe pulses.

As expected, the forward transmitted optical probe signal remains unchanged when the water cell is empty [Fig. 2(a)]. This indicates that the focused laser beam does not modify the glass forming the water container. As soon as the water cell is filled, the probe beam signal gets attenuated for a typical time period of 4 μ s [Fig. 2(b)]. We observed that in the absence of the pump beam, the probe beam signal remains unaffected which validates the fact that the probe beam does not interact with water. The events described in Fig. 2(b) are observed for repetition rates up to 142 kHz [as can be seen in Fig. 2(c)]. Above this value, the probe beam signal becomes unstable and chaotic, which indicates cumulative effects.

To interpret and validate the optical probe beam signals, a stroboscopic imaging setup is introduced along the axes orthogonal to the laser propagation. It consists of a pulsed light-emitting diode (LED; central wavelength is 447.5 nm, power is 0.5 W, Luxeon Philips), which is turned on for 1 μ s at various frequencies. Both the LED driver (Gardasoft PP860C) and the AOM (that drives the pump beam at a desired repetition rate) are synchronized using a

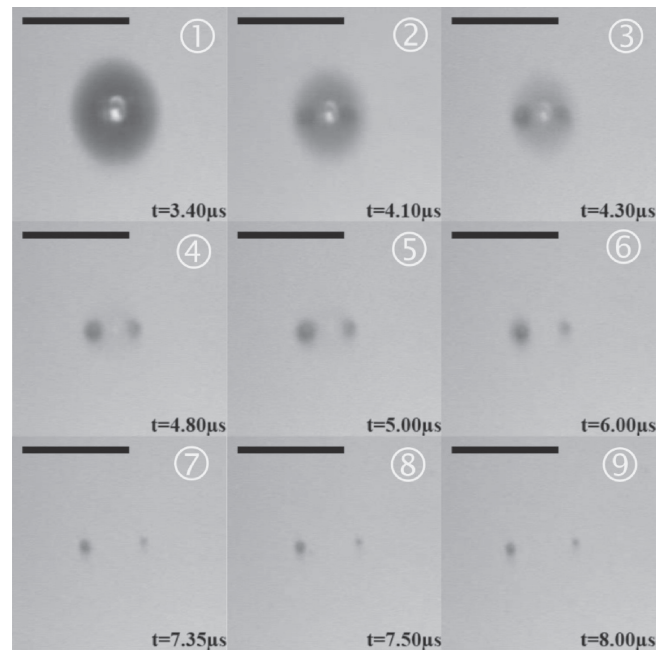


Fig. 3. Stroboscopic time-series images of femtosecond-laser (1 Hz repetition rate)-generated bubble close to the collapse phase (from 3.4 up to 8 μ s, the scale bar at the top of each image indicates 50 μ m). The integration time for the image formation is 1 μ s. (Note that the laser propagates from the right to the left of the images.)

signal generator (HP-33120a). With this method, the delay between the pump pulse and the lighting has a minimum value of $3.4 \mu\text{s} \pm 100 \text{ ns}$ (note that this minimum delay time is a limit set by our equipments). The camera (Sony XC-75 CE) is kept under asynchronous continuous operation at 25 Hz. To form the images (shown in Fig. 3), a $20\times$ magnification telecentric-lens (Moritex-Schott SOD-10X+2X) with a working distance of 5.5 cm is used. With this stroboscopic setup, the laser affected zone is imaged at different time stamps from 3.4 μ s onwards after the arrival of the pump pulse. Figure 3 shows a sequence of images taken at various time delays from 3.4 to 8 μ s. Each captured image was exposed to the LED light during 1 μ s.

The information collected with the probe beam signal combined with the stroboscopic images indicates that the laser–fluid interaction leads to two distinct regimes:

- I. From 0 to 4 μ s: bubble nucleation, expansion, and collapse at the focal spot.
- II. From 4 μ s onwards: no more distortions of the probe signal. Interestingly, we note the presence of two small bubbles still visible after 8 μ s. These tiny satellite bubbles do not produce any signal distortion in the probe signal. This observation illustrates the importance of a dual-monitoring system that includes a probe signal coupled with visual observations.

In the images obtained at 3.4 up to 4.3 μ s (images 1 to 3 in Fig. 3), the large circular dark spot is interpreted as the laser-induced bubble (we call this bubble “parent bubble”). Surprisingly, the images show highly spherical bubble formation at $t = 3.4 \mu\text{s}$ (given our low NA focusing objective lens). From the image 4.1 μ s onwards, the parent bubble vanishes while a pair of small dark spots (see at the

equator of the “parent bubble”) becomes prominent. We interpret these two smaller spots as bubbles that we call “daughter bubbles”. One should note that the events happening in the focal region are so fast that each image captures in fact overlapping events within 1 μs , the effective exposure time of the charge-coupled device (CCD). Therefore, the images may contain information related to multiple events depending on their time scale. This is particularly visible for the image taken at $t = 4.3 \mu\text{s}$ (image 3 in Fig. 3) where both parent and daughter bubbles are visible. From these observations, we conclude that the relevant regime for the parent bubble dynamics lasts up to 4 μs as evidenced in Figs. 2(b) and 2(c).

The strobe images taken at 4.1 μs and onwards show that the daughter bubbles are the key remnant features of the collapsing event. As time elapses after their formation, they shrink and move away from one another. This can be understood by estimating the Laplace pressure (i.e., the pressure difference between the inside and outside of a bubble due to surface tension²⁸). At $t = 5 \mu\text{s}$ and for a bubble radius of $R = 4.5 \mu\text{m}$, it turns out to be $P = 2\sigma/R \approx 32 \text{ kN/m}^2$ (or 0.316 atm, given σ as the surface tension = $71.97 \times 10^{-3} \text{ N/m}$ for water at 25 °C). Considering the atmospheric pressure and the Laplace pressure, we deduce that the vapor pressure is not sufficiently high to prevent the bubble from shrinking ($P_v < 1.316 \text{ atm}$).

To estimate the maximum bubble size, we consider the Rayleigh radius (R_{max})²⁸ at $t_c = 2 \mu\text{s}$, corresponding to half of the time duration over which the probe signal attenuates as seen in Figs. 2(b) and 2(c). This radius is given by

$$R_{\text{max}} = 1.01 \times t_c \sqrt{\frac{P_0 - P_v}{\rho_w}} = 22.34 \mu\text{m},$$

where P_0 is the ambient pressure far away ($P_0 = 1.05 \times 10^5 \text{ Pa}$), P_v is the vapor pressure in the bubble and ρ_w the density of water ($\rho_w = 1.0 \times 10^3 \text{ kg/m}^3$). This value is close to the measured radius $R_{3.4\mu\text{s}} = 23 \mu\text{m} \pm 2 \mu\text{m}$ measured at $t = 3.4 \mu\text{s}$. Although the Rayleigh radius estimate is based on unrealistic assumptions (it ignores the surface tension, thermal effects, and gas content of the bubble²⁸), it gives nevertheless reasonable estimates as pointed out in^{9,10,27–29}. This observation supports the fact that the main bubble collapses from $t = 3.4 \mu\text{s}$ onwards. Furthermore, we also observe a dependence of the bubble radius with the pulse energy. This observation was also reported by Aglyamov *et al.*²⁷ who used an ultrasound measurement technique to estimate the bubble radius.

The stroboscopic images from 4.1 to 6 μs (images 2 to 6 in Fig. 3) show “twin daughter” bubbles appearing near the focal region, which correspond to effective times (due to the 1 μs integration time) of 5.1 to 7 μs . (Note that after 6 μs —images 7 to 9 in Fig. 3, the twin daughter bubbles are still distinguishable but are much smaller and have moved away from the interaction zone.) In order to avoid the presence of daughter bubbles in the focal region, there has to be a minimum of 7 μs between two consecutive laser pulses, which corresponds to a frequency of 142 kHz. Indeed, we observe a loss of stability in the probe-beam at this repetition rate. This fact suggests that the system becomes chaotic due to the interaction of incoming pump pulses with the remnant twin-bubbles.

In conclusion, using a single-laser-source pump/probe setup combined with stroboscopic imaging, the collapse dynamic of a single femtosecond laser pulse-induced bubble was observed. The Rayleigh estimate of the maximum bubble radius shows a good agreement with the experimentally measured value. We have observed the appearance of twin daughter bubbles forming after the collapse of the main bubble. These twin bubbles trigger cumulative effects at a repetition rate above 142 kHz leading to an unstable bubble nucleation regime. This value sets the upper limit for femtosecond laser-induced droplet generation using bubble cavitation.

Acknowledgments This work is supported through the joint TU/e (Mechanical Engineering Dept)/TNO Holst Centre printing of conducting structures program. We thank Willie ter Elst and Eric Homburg for stimulating discussions and technical support throughout this work and A.J.M. Pemen for lending the oscilloscope for the probe signal measurements.

- 1) N. Bloembergen: *Nonlinear Optics* (World Scientific, Singapore, 1996) 4th ed., p. 121.
- 2) C. B. Schaffer, N. Nishimura, E. Glezer, A. Kim, and E. Mazur: *Opt. Express* **10** (2002) 196.
- 3) C. B. Schaffer: Ph. D. Thesis, Harvard University (2001).
- 4) A. Vogel, J. Noack, G. Hüttman, and G. Paltauf: *Appl. Phys. B* **81** (2005) 1015.
- 5) A. Vogel, S. Busch, and U. Parlitz: *J. Acoust. Soc. Am.* **100** (1996) 148.
- 6) K. König, I. Riemann, P. Fischer, and K. J. Halbhauer: *Cell. Mol. Biol. (Noisy-le-grand)* **45** (1999) 195.
- 7) V. Venugopalan, A. Guerra, K. Nahen, and A. Vogel: *Phys. Rev. Lett.* **88** (2002) 078103.
- 8) D. Lohse: *Nonlinear Phenom. Complex Syst. (Minsk)* **9** (2006) 125.
- 9) A. Vogel, N. Linz, S. Freidank, and G. Paltauf: *Phys. Rev. Lett.* **100** (2008) 038102.
- 10) J. Noack, D. X. Hammer, G. D. Noojin, B. A. Rockwell, and A. Vogel: *J. Appl. Phys.* **83** (1998) 7488.
- 11) D. Bartolo, C. Josserand, and D. Bonn: *Phys. Rev. Lett.* **96** (2006) 124501.
- 12) V. Duclaux, F. Caillé, C. Duez, C. Ybert, L. Bocquet, and C. Clanet: *J. Fluid Mech.* **591** (2007) 1.
- 13) S. T. Thoroddsen and A. Q. Shen: *Phys. Fluids* **13** (2001) 4.
- 14) J. R. Royer, E. I. Corwin, A. Florin, M.-L. Cordero, M. L. Rivers, P. J. Eng, and H. M. Jaeger: *Nat. Phys.* **1** (2005) 164.
- 15) M. S. Longuet-Higgins: *J. Fluid Mech.* **127** (1983) 103.
- 16) M. S. Barrow, S. W. J. Brown, S. Cordy, P. R. Williams, and R. L. Williams: *J. Fluids Eng.* **126** (2004) 162.
- 17) A. Antkowiak, N. Bremond, S. Le Dizes, and E. Villermaux: *J. Fluid Mech.* **577** (2007) 241.
- 18) H. E. Potts and D. A. Diver: *New J. Phys.* **3** (2001) 7.
- 19) A. Pearson, E. Cox, J. R. Blake, and S. R. Otto: *Eng. Anal. Boundary Elem.* **28** (2004) 295.
- 20) E. A. Brujan, G. S. Keen, A. Vogel, and J. R. Blake: *Phys. Fluids* **14** (2002) 85.
- 21) M. Duocastella, J. M. Fernández-Pradas, J. L. Morenza, D. Zafra, and P. Serra: *Sens. Actuators B* **145** (2010) 596.
- 22) I. Zergioti, A. Karaiskou, D. G. Papazoglou, C. Fotakis, M. Kapsetaki, and D. Kafetzopoulos: *Appl. Phys. Lett.* **86** (2005) 163902.
- 23) M. Colina, M. Duocastella, J. M. Fernández-Pradas, P. Serra, and J. L. Morenza: *J. Appl. Phys.* **99** (2006) 084909.
- 24) M. Duocastella, J. M. Fernández-Pradas, J. L. Morenza, and P. Serra: *J. Appl. Phys.* **106** (2009) 084907.
- 25) P. Serra, J. M. Fernández-Pradas, F. X. Berthet, M. Colina, J. Elvira, and J. L. Morenza: *Appl. Phys. A* **79** (2004) 949.
- 26) J. M. Fernández-Pradas, M. Colina, P. Serra, J. Domínguez, and J. L. Morenza: *Thin Solid Films* **453–454** (2004) 27.
- 27) S. R. Aglyamov, A. B. Karpiouk, F. Bourgeois, A. Ben-Yakar, and S. Y. Emelianov: *Opt. Lett.* **33** (2008) 1357.
- 28) E. Brennen: *Cavitation and Bubble Dynamics* (Oxford University Press, New York, 1995) p. 56.
- 29) A. B. Karpiouk, S. R. Aglyamov, F. Bourgeois, A. Ben-Yakar, and S. Y. Emelianov: *J. Biomed. Opt.* **13** (2008) 034011.